Construction and Building Materials 364 (2023) 129960

Contents lists available at ScienceDirect

Construction and Building Materials

journal homepage: www.elsevier.com/locate/conbuildmat

Experimental characterization of the nonlinear thermomechanical behaviour of refractory masonry with dry joints

Mahmoud Ali [a], Rafael L.G. Oliveira [b], João M. Pereira [c,*], João P. Rodrigues [e,f,g], Paulo B. Lourenço [c], Hans Ulrich Marschall [d], Thomas Sayet [a], Alain Gasser [a], Eric Blond [a]

[a] LaMé Laboratory (EA 7494), Université d'Orléans, Université de Tours, INSA Centre Val-de Loire, 8 rue Léonard de Vinci, 45072 Orléans, France
[b] University of Coimbra, ISISE, Department of Civil Engineering, Coimbra, Portugal
[c] University of Minho, ISISE, Department of Civil Engineering, Guimarães, Portugal
[d] RHI Magnesita, Technology Center, Leoben, Austria
[e] University of Coimbra, CERIS, Department of Civil Engineering, Coimbra, Portugal
[f] Itecons, Coimbra, Portugal
[g] Federal University of Minas Gerais, Department of Structural Engineering, Belo Horizonte, Brazil

ARTICLE INFO

Keywords:
Refractories
Masonry
Creep
Stress relaxation
Dry joints
High temperature tests

ABSTRACT

Refractory linings can withstand severe working conditions and are widely used for the linings of many high temperature applications, such as steel ladles. Some of these linings are built with dry joints. These structures undergo very complex responses in service conditions, making the prediction of its behaviour a challenging task. To develop robust numerical prediction tools, experimental validation is necessary. The present paper gathers a considerable database on the mechanical and thermomechanical characterization of refractory masonry with dry joints (up to 1500 °C). The test setups, measurement techniques, specimens, test procedures, and results of the large-scale experimental campaign are presented. The results of the tests help in understanding the complex thermomechanical behaviour of refractory linings. Aspect such as joints closure and reopening, dimensional and shape tolerances of the bricks, creep and stress relaxation are investigated. The results of these tests are essential for developing, calibrating, and validating efficient numerical models for the design and optimization of refractory masonry linings.

1. Introduction

Masonry systems with dry joints (*i.e.,* without mortar) are composed of stacked units (*e.g.,* bricks). There are different types of masonry assemblies, according to the function they aim to pursue. The most common use is in civil engineering applications. These are usually working and characterized under room temperature [1], and possibly fire conditions [2]. One other major use of this type of system is in heavy industries, specifically for high temperature industrial applications (higher than 1000 °C) [3–5]. The main difference between these two applications is the units constituting the assembly. In the former, the units are usually stones, fired clay, concrete, etc. [6], while in the latter, units are bricks made of refractory ceramics [4,7,8].

Owing to their high thermomechanical, thermal, and chemical stability, refractory ceramics can withstand severe working conditions including: high operating temperature (above 1000 °C), thermal shock, high thermomechanical stresses, erosion and corrosion which are identified as the main ageing factors of these materials [9–12]. Refractories are identified as advanced ceramics [13]. These materials are widely used for the linings of many high temperature applications, such as steel ladles, furnaces and rotary kilns, used in several heavy industries such as glass production, cement, iron and steel making [14–17].

In a typical refractory masonry lining with dry joints, bricks with height (h_b), width (l_b) and depth (d_b) are periodically arranged in running bond texture. Dry joints with initial thickness ($0 \leq g_0 \ll h_b; l_b; d_b$) separate the bricks from each other (Fig. 1). Often, these joints' thickness is a result of the surface unevenness, shape, and dimensions tolerances of the bricks during production. However, in some applications such as rotary kilns and blast furnaces, the joints' thickness is designed using cardboard spacers between the bricks during installation to compensate for thermal expansion effects [18]. Two types of joints are defined based on their orientation: bed joints (continuous horizontal

* Corresponding author.
E-mail address: jpereira@civil.uminho.pt (J.M. Pereira).

https://doi.org/10.1016/j.conbuildmat.2022.129960
Received 2 September 2022; Received in revised form 7 November 2022; Accepted 2 December 2022
Available online 8 December 2022

joints) and head joints (staggered vertical joints), see Fig. 1. The design and optimization of these linings is still an engineering challenge due to the complex interactions between the thermal fields, the chemistry and the nonlinear thermomechanical behaviour of refractories at high temperatures [15,19,20]. Therefore, additional research and development on refractory linings is required to meet existing and new demanding requirements in industries with high temperature processes.

Previous experimental studies on refractory masonry with dry joints focused on small-scale tests, with only a few references on large-scale tests. The first usually uses a few bricks to measure the dry joints thickness and contact area between the adjacent surfaces of the bricks, dimensional tolerances of the bricks and ultimate compressive strength of small assemblies of bricks. The second is used to gather data on the impacts of dimensional and shape tolerances, joints, joints closure and reopening on the global behaviour of the structure. These experimental studies are usually performed at room temperature and high temperature.

Andreev et al. [21] performed uniaxial compression tests at various temperatures to investigate the impact of joints on the mechanical behaviour of magnesia carbon cylindrical samples. Two types of samples were tested, namely: samples with one dry joint and samples without joints. The samples with joint showed nonlinear behaviour with progressive strain stiffening compared to samples without joints. The gradual closure of the joint is responsible for the non-linearity in the stress–strain curve, and it disappears when joints close (*i.e.*, the two cylindrical parts reach perfect contact).

Understanding joint closure behaviour can be assisted by using full-field measurement techniques such as digital image correlation (DIC). Allaoui et al. [22] performed uniaxial compression tests at room temperature of a stack of two magnesia chromite refractory bricks to investigate the local and global behaviour of dry joints. Their results demonstrated that joints' behaviour is heterogeneous, nonlinear, and orthotropic. The local joint opening was noticed (during compression) due to rigid body rotation of the bricks. In addition, the dimension tolerances of the bricks determine the joint thickness, while surface roughness is a complement. Similar results were obtained by Oliveira et al. [23].

The dimensional tolerances and surface roughness of the bricks lead to limited contact between the adjacent surfaces of the joints. This, in turn, leads to stress concentration and a decrease in the ultimate compressive strength of the assembly [23]. Several experimental studies were conducted to investigate the relationship between actual contact area and load bearing capacity of dry stack and running bond masonry systems and to test different strategies for mitigating dimensional errors and surface roughness of the bricks [21,24–26]. Usually, the contact area is measured using carbon paper [27], pressure-based sensors [24] or contact sensors [25].

Chewe Ngapeya and Waldmann [25,26] performed uniaxial compression tests of small masonry assemblies built up from three bricks to study the impact of contact area on the ultimate compressive strength of the masonry. Different contact layers were applied to the bed joint surfaces. The contact area was measured using contact sensors. Their results indicated that increasing the contact area from 23 to 98 % resulted in an improvement factor of 1.97 in terms of maximum failure load. Similar results were obtained by Zahra and Dhanasekar [24]. As reported by Andreev et al. [21] and later by Zahra [24], grinding the surfaces of joints is another efficient solution, as it leads to decreased surface unevenness, helping to attain perfect contact and, thus, increases the contact area and load bearing capacity of the structure.

Regarding large-scale tests, Prietl and Nguyen et al. [28–31] studied the mechanical behaviour of magnesia chromite refractory masonry with dry joints (1 × 1 m^2 assemblies) subjected to in-plane biaxial compression load at room temperature and at 1200 °C. The authors showed that the mechanical behaviour of the wall is orthotropic. Under the same applied load and for both, room and high temperature tests, the resulting strains in the direction normal to the surfaces of bed joints are higher than in the direction normal to the surfaces of head joints. The mechanical behaviour of the wall was found to be nonlinear due to gradual closure of joints and the increase of the effective stiffness with joints closure. When compared to the room temperature test and under the same applied load, the strains, in the two directions were higher due to the decrease of the material stiffness with increasing temperature and the viscoplastic behaviour of refractories at high temperature.

Recently, the mechanical behaviour of alumina spinel refractory masonry, in the direction normal to bed joints, at room and high temperatures (up to 900 °C) was experimentally investigated by Oliveira et al. [3]. Different loading conditions were investigated, including cyclic loading and thermal gradient. It was found that the mechanical behaviour of the walls was highly nonlinear with strain stiffening. The stiffness and ultimate compressive strength of the walls were smaller than those of the base material of the bricks. The stiffness of the wall increased with increasing applied load level. Moreover, the dimension and shape tolerances of the bricks led to stress concentrations and cracks in the middle of the bricks. They observed an ultimate compressive strength of 17.8 MPa at room temperature.

Creep (viscoplastic behaviour) is the time and temperature dependent deformation under constant stress [12]. A ceramic material subjected to constant stress at specific high temperature exhibits creep behaviour in three stages. Primary creep (time dependent strain rate), secondary creep (constant strain rate) and tertiary creep (increased strain rate till failure) [15,32,33]. Creep behaviour of alumina spinel brick at various temperature and stress level is researched for small specimens [15], however, the effect of creep behaviour at large-scale on a masonry is not evaluated.

It is clear from the studies presented above that the available literature on large-scale tests of refractory masonry with dry joints is limited,

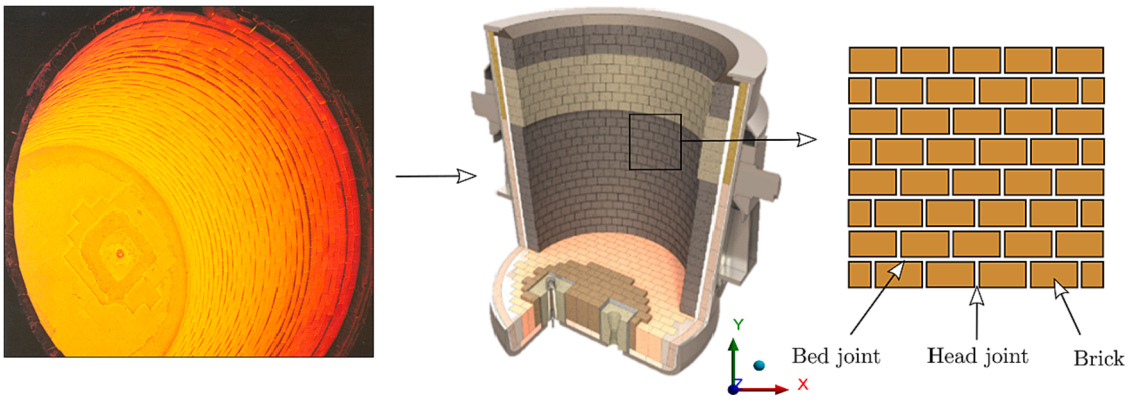

Fig. 1. Example of refractory lining applications in a steel ladle lined with refractory masonry with dry joints and a schematic representation of masonry lining showing the periodically arranged bricks and the joints [18].

with only 2 experimental campaigns. It should also be noted that the available tests at high temperatures were performed at 900 and 1200 °C, which is below normal operating conditions (around 1500 °C). Due to the complex behaviour of such applications at high temperatures, the need for additional experimental campaigns on large-scale assemblies is paramount. This work is devoted to the experimental characterization of refractory masonry walls subjected to uniaxial and biaxial compression loads at room and high temperatures. Within the framework of the ATHOR Network [34], two large-scale experimental campaigns were performed. Details regarding the first experimental campaign are reported elsewhere [3].

The second experimental campaign is presented here. The mechanical and thermomechanical behaviour of alumina spinel refractory masonry was investigated for various loading conditions at room and high temperatures up to 1500 °C. Large-scale uniaxial compression tests were performed in the directions normal to bed and head joints, and biaxial compression tests at room temperature. Large-scale uniaxial and biaxial creep tests, as well as biaxial relaxation tests were carried out at 1500 °C. Besides this section, this paper includes: *a)* in Section 2 a detailed description of the experimental setup; *b)* in Section 3 a description of the materials and specimens used in the experimental campaign; *c)* in Section 4 a summary of the experimental procedures, results, and discussion of the obtained results; *d)* finally, in Section 5, conclusions are drawn and presented.

2. Experimental setup

The experimental campaign presented in this work was performed at the Technology Centre Leoben (TCL) of RHI-Magnesita, in Austria. The experimental setup has been used before [30] and it was upgraded considering this experimental campaign (Fig. 2). The test setup consists of: *a)* a monolithic reaction frame in which the hydraulic jacks, LVDTs and heating system were connected; *b)* two orthogonal hydraulic jacks with the capacity of 1000 kN, with a Rexroth controller unit; *c)* a Eurotherm 5180 V 48-channel data acquisition system.

Detailed views of the 3D model of the test field at room and high temperatures are presented in Fig. 3a and b. The reaction frame has sufficient stiffness so that during testing, the displacements in the frame do not impact the measured displacements in the specimen. Two hydraulic cylinders, with maximum stroke of 90 mm, were used and each cylinder was equipped with two pressure gauges for measuring the applied forces. The temperatures of the cylinders were monitored during the tests to ensure safe operating temperature.

Four steel plungers were used for the boundary conditions of the specimen, two of them are fixed, and the others are movable. The two movable plungers were connected to hydraulic cylinders and equipped with lateral steel guides to ensure their alignment during load application. The lateral guides were lubricated to reduce friction. All plungers were water-cooled to avoid overheating the hydraulic cylinders during tests performed at high temperatures. Each fixed plunger has three openings for placing the measurement instrumentation (LVDTs and thermocouples). To protect the plungers, these were lined with Magnesia Chromite (MCh) refractory bricks with dry joints. MCh bricks were chosen due to their high elastic stiffness and creep resistance. Dry joints were chosen to allow free expansion of the MCh bricks during high temperature tests.

The specimen rests on top of four insulation layers of refractory masonry. The top layer (in contact with the specimen) was masonry with dry joints, while the other three layers were masonry with mortar joints. The number of layers, material and thickness of each layer were chosen based on several heat transfer numerical simulations. For the tests at high temperatures, a heating hood equipped with 36 KANTHAL SUPER 1900 heating elements was used. The heating hood was composed of steel frame and 20 cm thickness insulation. The maximum operating temperature of the heating elements was 1850 °C.

2.1. Displacement measurement

For measuring the in-plane displacement of the specimen, four adapted LVDT devices were used (Fig. 4). Each device was composed of: *a)* LVDT (Fig. 4c) with ± 50 mm range, placed inside a steel tube; b) a steel and alumina tube glued together using high temperature glue (Fig. 4b); and *c)* a long alumina tube with one open end, installed inside the alumina and steel tubes and touching the LVDT tip (Fig. 4a). The objective is to protect the LVDT from the high temperatures inside the testing area. This arrangement was used so that the materials used do not influence the measured displacements under high temperatures. A thermocouple is installed in the long alumina tube for monitoring.

In addition to the LVDTs, Digital Image Correlation (DIC) was used to measure the full displacement fields in room temperature tests. One 18-megapixel (5184 × 3486) camera was used to take pictures of the wall. LED lights were used to improve the contrast of the images. The bricks were laid on the floor and the speckle pattern was generated using black automotive paint and a brush. Finally, the bricks were left to dry for 48 h before the test. After the test, open-source software (Ncorr) was used for the DIC analysis [35].

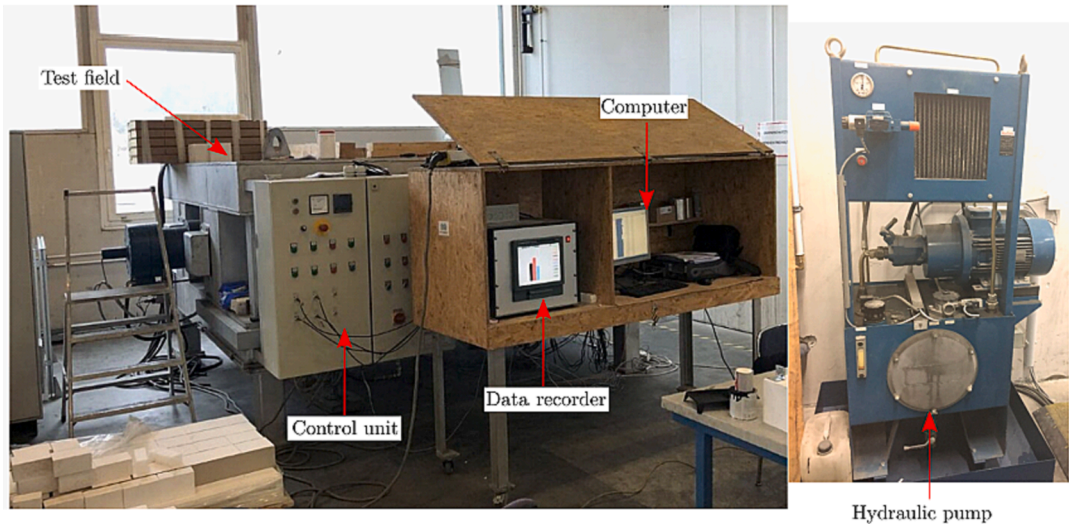

Fig. 2. Biaxial compression test setup at the Technology Centre Leoben (TCL) of RHI-Magnesita, Austria.

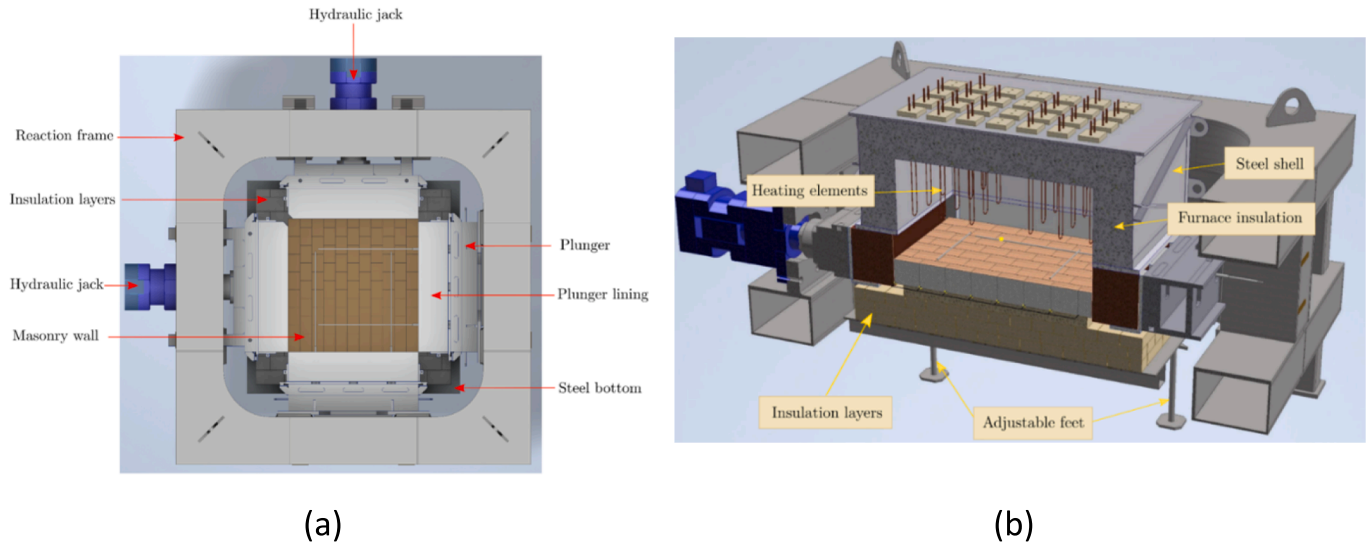

Fig. 3. 3D schematic model of biaxial compression test setup: a) top view; b) cross-section view showing the heating chamber, the test specimen, the metallic and ceramic plungers, and the insulation layers.

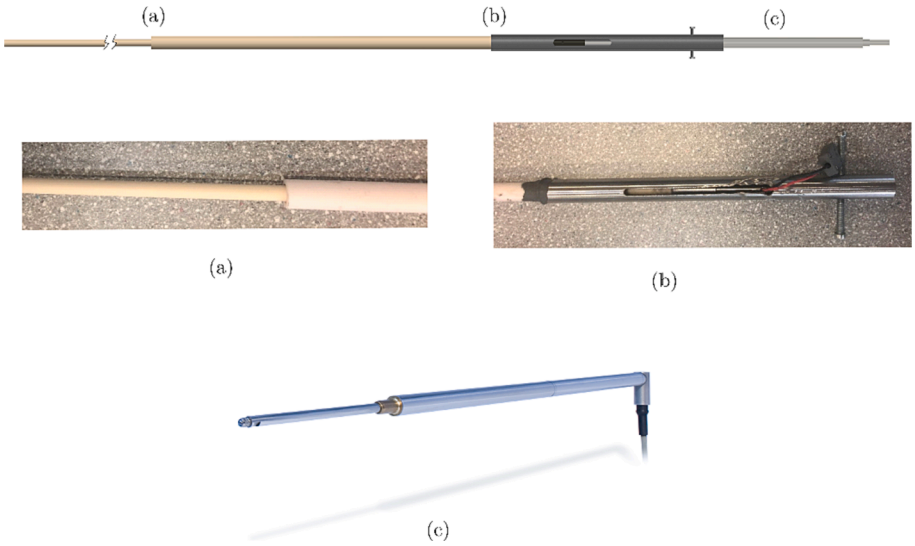

Fig. 4. Details of the LVDT device used to measure the displacement and temperature: a) corundum tube; b) steel tube; c) LVDT.

2.2. Temperature measurement

To measure the temperature during the tests, several thermocouples were used at different locations. Five type B thermocouples were used to measure the temperature of the cold face of the specimen (Fig. 5). Five type B thermocouples were used to measure the temperature of the hot face of the specimen, four of them placed in the LVDT tubes and the other one in direct contact with the hot face. One type S thermocouple was used to measure the air temperature inside the heating hood. Eleven type K thermocouples were used to monitor the temperature of the LVDTs, hydraulic cylinders, steel bottom frame and steel plungers.

3. Specimens

The specimens studied within this work were composed of alumina spinel bricks. The base material of the bricks has been fully characterized within the ATHOR Network. The chemical composition of the material is 94 wt% alumina, 5 wt% magnesia and 1 wt% other oxides such as iron oxide and silica. The apparent porosity and density of the material are 19 % and 3130 kg/m^3, respectively [15]. The thermal conductivity and specific heat of the material are shown in Fig. 6a and b [36]. The Young's modulus, and the ultimate compressive stress [23] variations with temperature are presented in Fig. 6c and d, respectively. The coefficient of thermal expansion of the material is 8.87 $\times$ 10^{-6} K^{-1} [37].

Full and half bricks were used in a running bond texture to build the specimens. The dimensions of the full bricks were 150 $\times$ 100 $\times$ 140 mm^3 (length, height, and depth). The dimensional tolerances of the bricks were $\pm$ 2 mm in the pressing direction (150 $\pm$ 2 mm) and $\pm$ 1 mm in the directions normal to the pressing direction (100 $\pm$ 1 mm and 140 $\pm$ 1 mm). The tolerance in the pressing direction is higher as dimensions are affected by the amount of powder material injected in the mould and the applied pressure during the production process. The dimensional and shape tolerances of the bricks lead to non-uniform joint thickness in the wall and limited initial contact. As seen in Fig. 7, the dry joints were almost closed at some locations while being open at others.

Thirteen compression tests of alumina spinel refractory masonry walls were performed. Six were carried out at room temperature, and

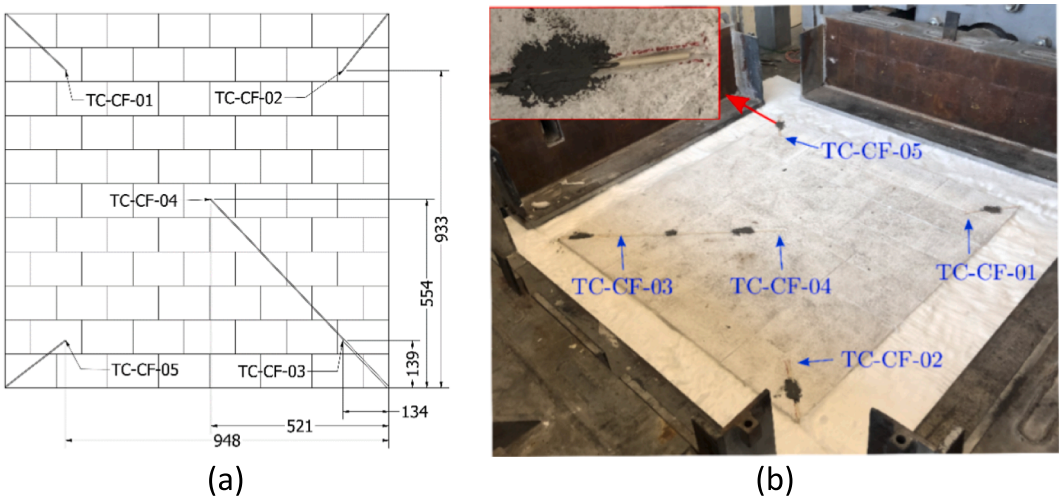

Fig. 5. Location of thermocouples for the cold face: a) schematic plan view, all dimensions are in mm; b) thermocouples in place.

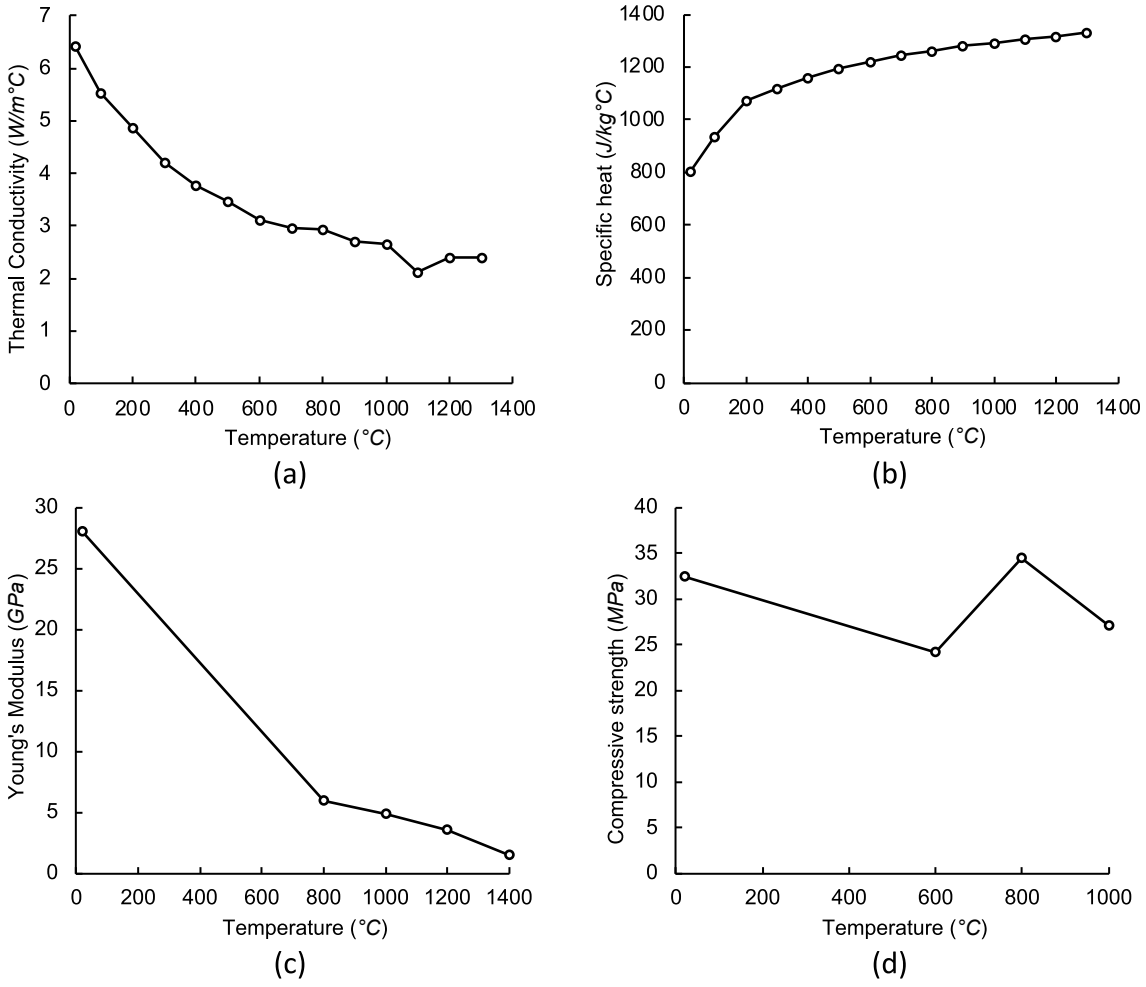

Fig. 6. Thermal and mechanical properties of alumina spinel bricks tested in the present work: a) thermal conductivity [34]; b) specific heat [34]; c) Young's modulus [35] and; d) ultimate compressive strength [16].

the remaining seven tests were performed at high temperatures. The test series names and loading conditions are given in Table 1. For all tests, the dimensions of the walls were 1125 × 1100 × 140 mm^3. It should be noted that the maximum load applied in this campaign is limited by the hydraulic jacks' capacity and safe operating temperature.

Schematic representations of the specimens, including their dimensions, bricks' arrangements, and locations of the LVDTs for the seven-test series are given in Fig. 8 and Fig. 9. Fig. 10a shows an example of the specimen before testing, referring to S03 (at room temperature). Fig. 10b shows an example of the specimen before testing, referring to

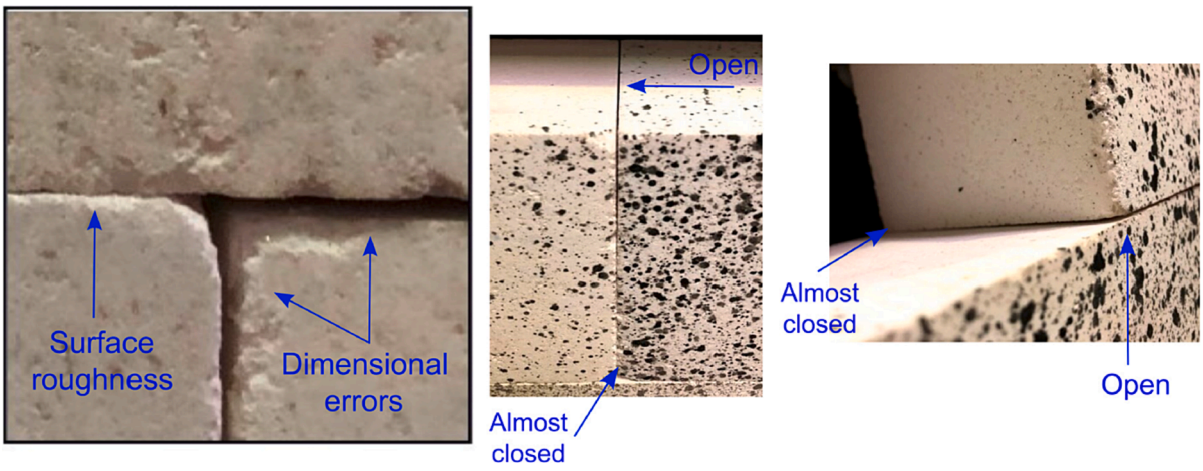

Fig. 7. Nonuniform dry joints thickness and limited initial contact caused by the dimensional and shape tolerances of the bricks.

Table 1
Summary of the biaxial compression tests of refractory masonry walls performed at room and high temperatures.

Series	Specimen	Maximum load		Temperature
		⊥ to bed joints	⊥ to head joints	
S01	S01 – 01	6 MPa	Constrained	Room temperature
	S01 – 02			
S02	S02 – 01	Constrained	6 MPa	
	S02 – 02			
S03	S03 – 01	6 MPa	6 MPa	
	S03 – 02			
S04	S04 – 01	4 MPa	Constrained	High temperature
	S04 – 02			
S05	S05 – 01	Constrained	4 MPa	
S06	S06 – 01	4 MPa	4 MPa	
	S06 – 02			
S07	S07 – 01	4–6 MPa	4–6 MPa	
	S07 – 02			

S06 (at high temperature). For the tests at high temperatures, special attention was given to the insulation of the testing area. As can be seen in Fig. 10b, several layers of ceramic wool were used to limit the heat losses.

4. Test procedures, results, and discussions

The experimental results are presented and discussed in this section. For each test series, results in terms of displacements, forces, and temperatures are presented and discussed. Wherever possible, comparisons with literature results are made.

The testing procedures for the room temperature tests were: *(i)* The speckle pattern was applied to the bricks. *(ii)* The wall was built in the testing field. *(iii)* The LVDTs were connected and calibrated, and the camera was placed in front of the wall, its correct alignment was verified. Then, several reference images were taken. *(iv)* The moving plungers (normal to bed or head or both joints, depending on the test series) were moved until they touched the wall sides. *(v)* The load was applied to the wall under displacement control (0.01 mm/*sec*). The displacements and reaction forces were recorded. *(vi)* After reaching the maximum load, a dwell time of around 100 s was considered. Then, unloading, under displacement control, was performed.

Regarding the high temperature tests, the testing procedures were: *(i)* The wall was built in the testing field, and ceramic insulation (super wool) was placed on top of the moving and fixed plungers. *(ii)* The LVDTs and thermocouples were connected, calibrated, and the water-cooled system of the plungers was turned on. *(iii)* The heating hood was placed on top of the test field and heating started. The temperatures of the cold and hot faces were recorded. *(iv)* After reaching thermal steady state, the moving plungers (normal to bed or head or both joints, depending on the test series) were moved until they touched the wall. *(v)* The load was applied under displacement control (0.01 mm/*sec*) till reaching the required loading level. Then the hydraulic cylinder controller was switched to force or displacement control (force control in creep tests and displacement control in relaxation tests) during the holding time and, finally, unloading.

4.1. S01: Uniaxial loading and unloading - normal to bed joints at room temperature

The main objective of series S01 was to investigate the impact of joints closure and reopening on the mechanical response of the wall when subjected to cyclic loading at room temperature in the direction normal to bed joints. It should be noted that while a force was being applied in the direction normal to the bed joints (6 MPa), the direction

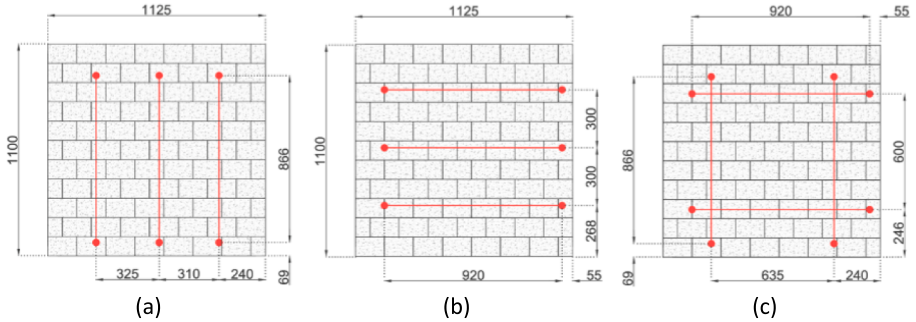

Fig. 8. Schematics of the specimens tested at room temperature showing the arrangements of the bricks and LVDTs: a) S01; b) S02; c) S03. Dimensions in mm.

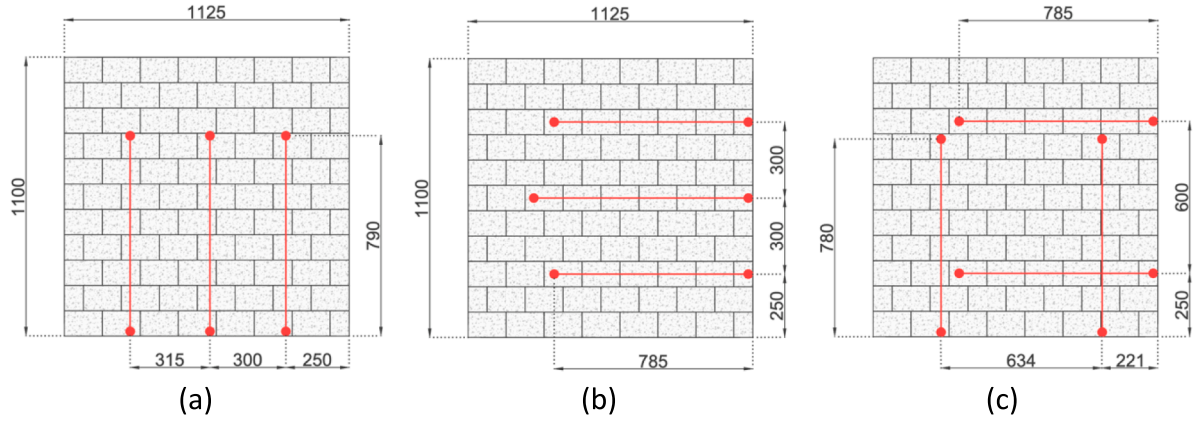

Fig. 9. Schematics of the specimens tested at high temperature showing the arrangements of the LVDTs, bricks and the dimensions of the walls: a) S04; b) S06 and S07; c) S05. Dimensions in mm.

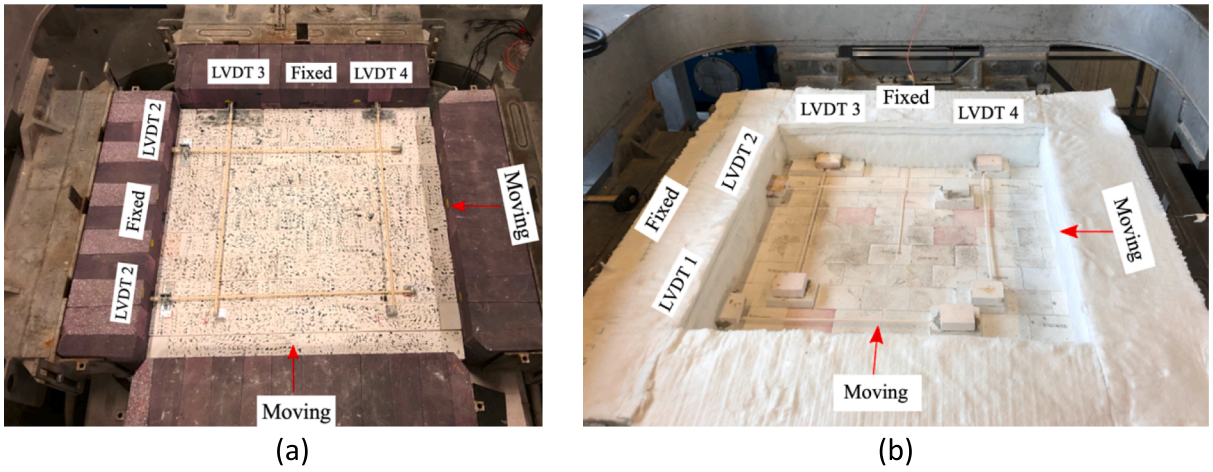

Fig. 10. Example of specimens before testing: a) at room temperature (S03); b) at high temperatures (S06).

normal to the head joints was constrained by the plungers (*i.e.*, the positions of the plungers were locked).

An example of the recorded reaction forces normal to bed (f_{bed}) and head (f_{head}) joints during loading and unloading is given in Fig. 11a. During loading, f_{bed} increased gradually to reach the pre-programmed maximum value of 945 kN. Then, f_{bed} remained constant during a dwell period to capture images at peak load. Afterwards, the unloading stage started, and the measured reaction force dropped gradually.

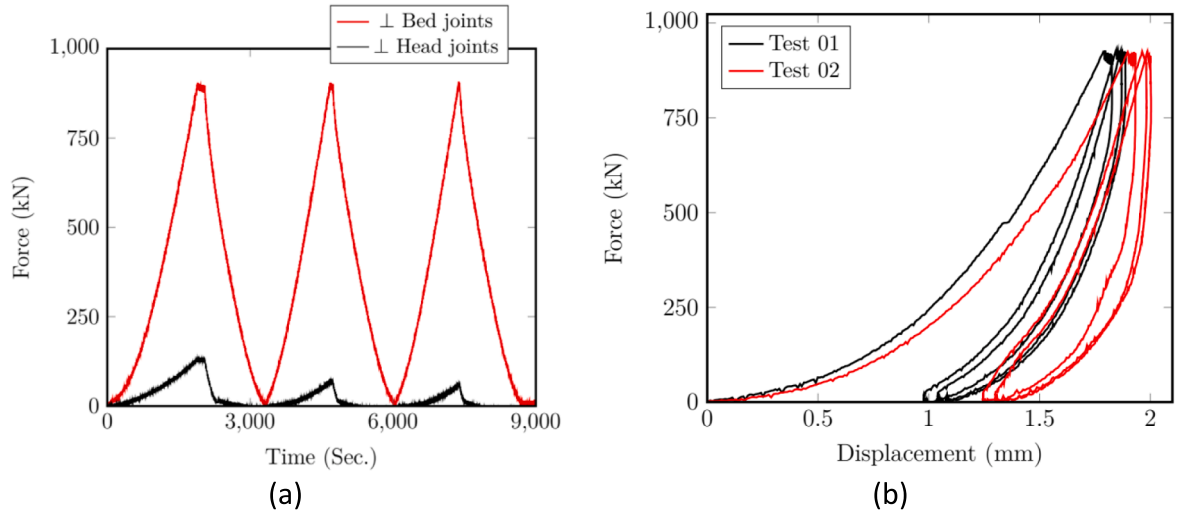

Fig. 11. Series S01: a) measured reaction forces in directions normal to the surfaces of bed and head joints during loading and unloading; b) force–displacement diagram in the direction normal to bed joints.

Finally, the first loading/unloading cycle was repeated two times. The behaviour of the f_{head} followed the trend of the f_{bed}, caused by the constrained expansion of the wall in the direction normal to the head joints. It should be noted the difference between f_{bed} and f_{head} when unloading. Here, f_{head} dropped to zero in a shorter period than $f_{bed.}$ This can be attributed to the difference between the maximum values of f_{bed} and f_{head} before the unloading stage.

Force displacement diagrams of the two performed tests are shown in Fig. 11b. The displacements were calculated as the average of the displacements measured by the 3 LVDTs. The obtained results are consistent. Fig. 12 presents the full displacement fields obtained using DIC, in the direction normal to bed joints, for specimen S01-01 at different load levels. In agreement with the results obtained by Oliveira et al. [3], non-uniform displacement fields can be seen in the figure. Higher values of displacement at the right side of the wall can be observed. In addition, after unloading, permanent deformations could be noted, and the wall did not reach its initial configuration. This can be attributed to the fact that the final joint thickness after unloading is usually smaller than the initial one. This behaviour was also noticed from cyclic loading and unloading of a stack of two bricks [23].

During loading, a nonlinear displacement stiffening behaviour can be observed (see Fig. 11b). This behaviour was caused by the gradual closure of joints and increased stiffness with joints closure. Regarding unloading, in the beginning, a considerable drop in the reaction forces was noticed without any decrease in displacement. Then, both the displacement and reaction force decreased. The slope of the curve during unloading was steeper as compared to that of first loading step. This behaviour indicates that the joint behaviour during the loading step of the first cycle is different from the joint behaviour during unloading step of the first cycle and from the loading/unloading of the second and third cycles. During the first loading stage, the asperities, and the surface roughness at the contact surfaces of the bricks were crushed and/or deformed. Therefore, at the end of the loading stage, the joints were not the same as before loading.

4.2. S02: Uniaxial loading and unloading - normal to head joints at room temperature

Series S02 was performed in a similar way as S01 with uniaxial compression of 6 MPa applied normal to head joints. Due to technical issues related to the camera holding setup and some rigid body motions, DIC analysis were not successful for this test series.

Fig. 13a shows an example of the recorded reaction forces normal to head (f_{head}) and bed (f_{bed}) joints during loading and unloading. Compared to S01, the maximum pre-programmed force (924 kN) was reached in a shorter period due to less number of head joints in the wall (7 head joints and 10 bed joints). Afterwards, the unloading stage started, and the measured reaction forces dropped gradually. Finally, the first cycle was repeated two times. The behaviour of the f_{bed} followed the trend of the f_{head}, caused by the constrained expansion of the wall in the direction normal to the bed joints. It should be noted that the value of f_{bed} was smaller than f_{head} in the case of S01, because of the difference in the number of bed and head joints in the wall. A higher number of joints in the direction normal to the loading direction leads to more space to absorb the lateral expansion of the wall caused by Poisson's effects and, therefore, low values of resulting reaction forces.

Fig. 13b shows the force–displacement diagrams of the two performed tests. The displacements were calculated as the average of the displacements measured by the 3 LVDTs. Compared to S01, higher differences between the two tests can be observed. This can be caused by the higher tolerances in the length of the bricks as compared to the tolerances in the height of the bricks ($\pm$2 mm and $\pm$ 1 mm, respectively). A nonlinear displacement stiffening behaviour during load application, due to gradual closure of head joints, can be noticed from the figure. In comparison to S01, the maximum value of the average displacement measured by the LVDTs is smaller (1.3 mm for S02 and 2 mm for S01), because the number of head joints was less than the number of bed joints. This leads to higher stiffness in the direction normal to head joints as compared to the direction normal to bed joints. The unloading behaviour is similar to S01.

4.3. S03: Biaxial loading and unloading at room temperature

Series S03 was carried out to investigate the mechanical response of the wall under biaxial compression ($\sigma_{bed}/\sigma_{head} = 1$) at room temperature. Therefore, a 6 MPa biaxial compression load was applied to the directions normal to bed and head joints.

Fig. 14a shows an example of the evolution of the measured reaction forces normal to head (f_{head}) and bed (f_{bed}) joints during loading and unloading stages of the three performed cycles. From the previous uniaxial compression tests, it has been shown that the stiffness of the wall in the directions normal to bed and head joints is different. The displacement rate of the two moving plungers was adjusted to keep $f_{bed} / f_{head} = 1$. The maximum forces (945 and 924 kN) were reached almost simultaneously during loading. f_{bed} and f_{head} remained constant during the dwell period. Then, the unloading stage started, and the measured reaction forces dropped gradually. The first cycle was repeated two times.

Fig. 14b shows the force–displacement curves of the two specimens. The displacements in each direction are calculated as the average of the displacements measured. Good agreement between the two tests can be observed. During the load application stage, and for both directions, a nonlinear displacement stiffening behaviour, due to the gradual increase of stiffness with the gradual closure of joints, was observed. The maximum displacement in the direction normal to head joints is smaller

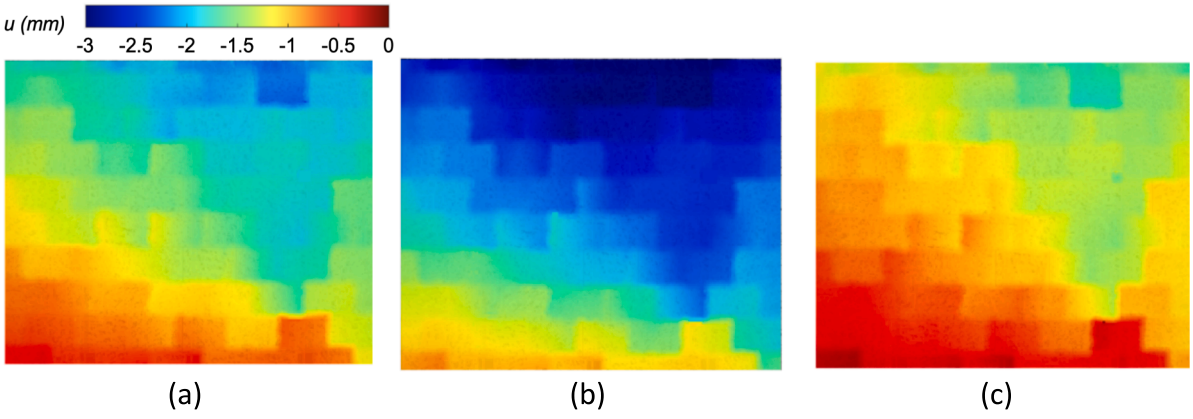

Fig. 12. Displacement fields for specimen S01-01, in the direction normal to bed joints (vertical direction in this image), at: a) 25 % of maximum load level; b) 100 % of maximum load level; c) after unloading.

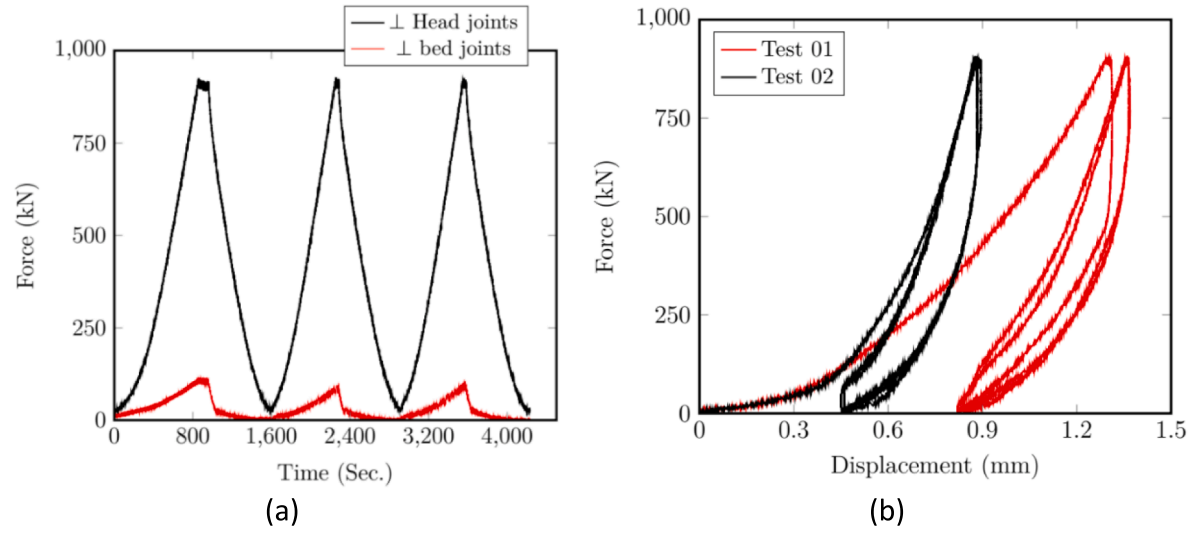

Fig. 13. Series S02: a) measured reaction forces in directions normal to the surfaces of head and bed joints during loading and unloading; b) force–displacement diagram in the direction normal to head joints.

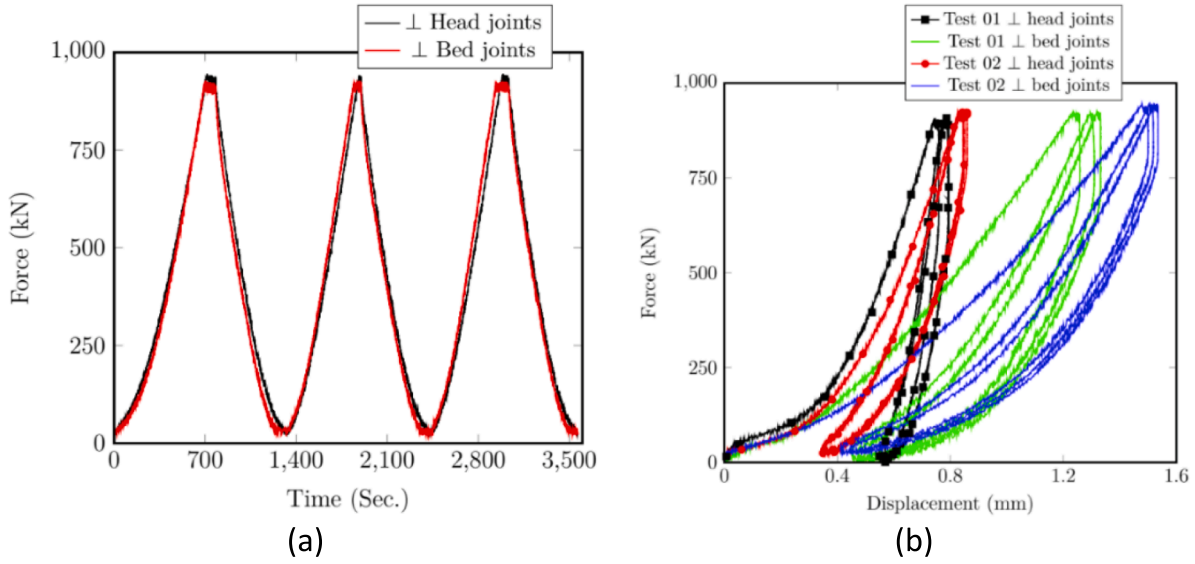

Fig. 14. Series S03: a) resulting reaction forces in directions normal to the surfaces of bed and head joints during loading and unloading; b) force–displacement diagrams in the directions normal to bed and head joints.

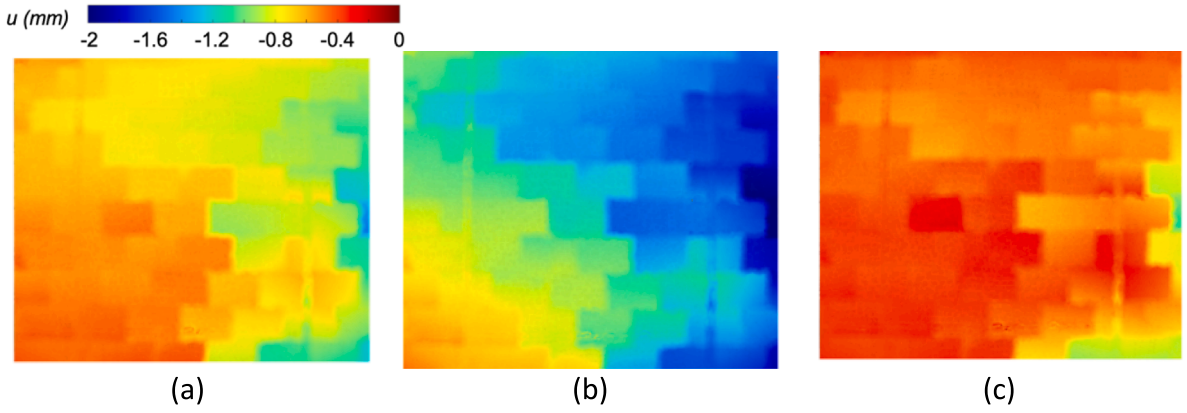

Fig. 15. Specimen S03-02: displacement fields in the direction normal to head joints (horizontal direction in the image) at: a) 25 % of maximum load level; b) 100 % of maximum load level; c) after unloading (first cycle).

when compared to the direction normal to bed joints, because the number of joints in each direction. Moreover, comparing with the maximum measured displacements in uniaxial tests (series S01 and S02), the maximum values of the average displacements (in both directions) measured in biaxial tests were smaller. This reduction could be caused by the shear interaction between bricks and the loading plungers. The unloading behaviour and the remaining cycles are similar to the previous series.

The full displacement fields obtained using DIC, for both directions and at different loading levels, for specimen S03-02 can be seen in Fig. 15 and Fig. 16. Some noise caused by the tubes for LVDTs can be seen in the images. Nonuniform displacement fields can be seen in these figures. The negative signs in the colour maps are due to the coordinate system used in DIC analysis. Absolute values should be considered when comparing the two DIC figures with the force–displacement diagrams.

4.4. S04: Uniaxial creep behaviour normal to bed joints

The main goal of series S04 was to understand the impact of bed joints, and bed joints closure on the nonlinear mechanical response (elastic viscoplastic behaviour) of the wall at high temperatures. Therefore, a 4 MPa uniaxial compression load was applied to the direction normal to bed joints and the sides of the walls were constrained by the locked plungers.

The defined heating procedure for all high temperature tests was: from 20 °C to 500 °C in 10 min then, from 500 °C to 1500 °C in 10 h. The temperature evolutions for the cold and hot faces during heating, mechanical load application, holding and unloading are presented in Fig. 17. The temperatures of the HF (hot face) and the CF (cold face) were measured using ten type B thermocouples, five in each face (Section 2.2). Similar temperature for all five thermocouples on the HF were obtained, indicating uniform temperature distribution. In the CF, the five solid black lines in the figure represent the temperatures measured by five thermocouples. The temperature of the CF centre was higher compared to four thermocouples installed near the corners of the wall. This is due to heat losses from the sides of the wall to the four ceramic loading beams. It took around 28 h to heat the specimen up to 1500 °C and reach thermal equilibrium. For all other test series presented below, similar temperature distributions were obtained.

While heating, the wall was free to expand. Then, a uniaxial compression load of 4 MPa (630 kN) was applied in the direction normal to the bed joints, while the direction normal to head joints was restrained by the plungers. Fig. 18 shows an example of the recorded reaction forces normal to bed (f_{bed}) and head (f_{head}) joints during loading, holding, and unloading stages. During loading (lasted around 50 min), f_{bed} rose gradually to reach the pre-programmed maximum value of 630 kN (4 MPa). Then, f_{bed} was kept constant during the load

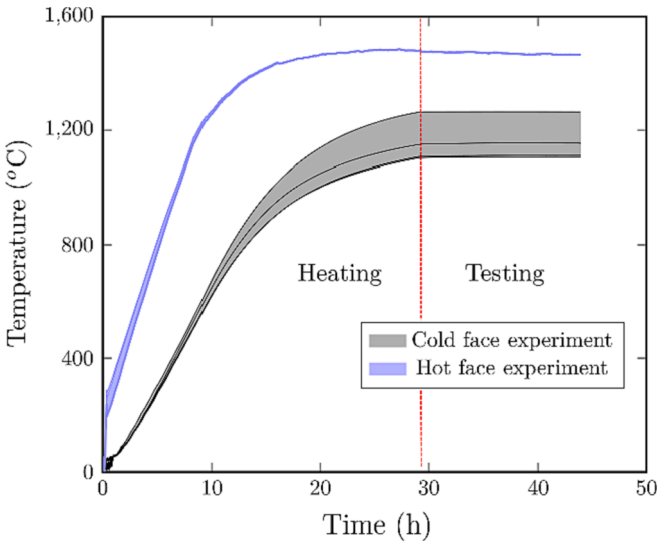

Fig. 17. Test series S04: temperature evolution of the cold and hot faces during heating and mechanical testing.

holding time (16 h). An increase in f_{head} was observed (to around 43 kN) with the increase of f_{bed}. This increase was caused by the lateral restraint provided by the locked plungers. During the beginning of the holding step, f_{head} decreased due to the relaxation behaviour in the direction normal to head joints (due to locked positions of the plungers in contact with the sides of the wall). Then, it remained constant at around 20 kN (smallest value that can be measured by the force sensors). Finally, during unloading, f_{bed} and f_{head} decreased gradually to zero.

Fig. 19 presents the resulting force–displacement diagrams and the displacement - time diagrams of the two specimens during all steps. Good agreement between the two tests was observed. A nonlinear displacement stiffening behaviour can be observed during the loading step. During the holding step, an increase in displacement can be observed due to creep. Then, the displacement decreased slightly due to unloading. Moreover, after load removal, the recovered strain was very small when compared to the strain due to the applied load. This can be attributed to the following: first, during unloading, only few joints reopened, and their final thickness was very small when compared to the initial joint thickness (additional details about this point will be given later in Section 4.8); second, the permanent deformation resulting from the viscoplastic behaviour of the structure. The noise in the measured force was caused by a problem in the controllers of the hydraulic jacks. By analysing the displacement - time diagrams, it is possible to observe the primary and secondary creep stages. The primary creep can be

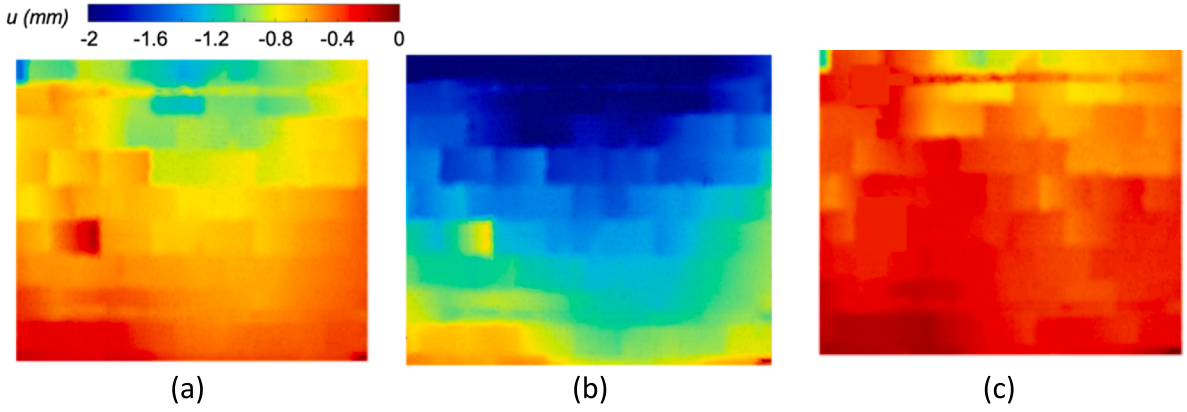

Fig. 16. Specimen S03-02: displacement fields in the direction normal to bed joints (vertical direction in the image) at: a) 25 % of maximum load level; b) 100 % of maximum load level; c) after unloading (first cycle).

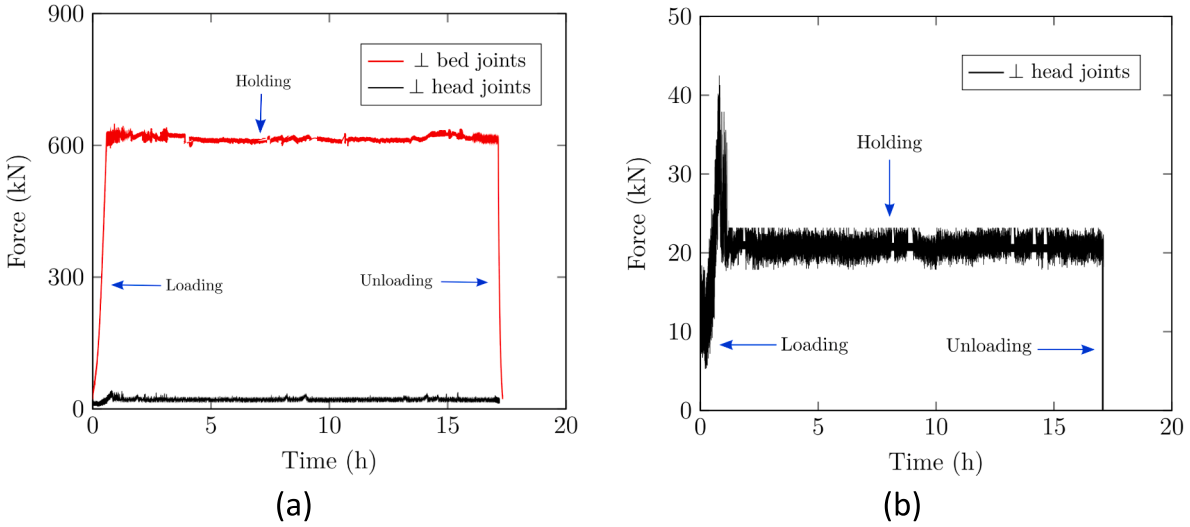

Fig. 18. Specimen S04-01: recorded reaction forces during mechanical loading, holding, and unloading stages: a) in the directions normal to the bed and head joints; b) in the direction normal to the head joints.

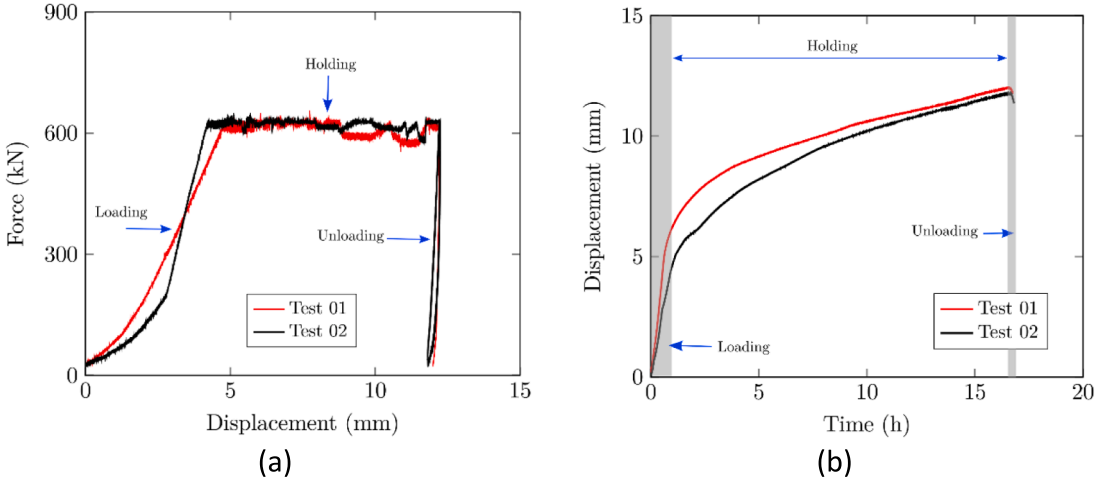

Fig. 19. Test series S04: a) resulting force–displacement diagrams; b) time variations of the average displacements during mechanical loading, holding, and unloading steps in the direction normal to bed joints.

characterised by the increasing strain rate till five hours of the holding and a constant strain thereafter till end of holding. The total strain ε_t in the wall by the end of load application step was around 0.005. This value reached 0.015 by the end of holding step.

4.5. S05: Uniaxial creep behaviour normal to head joints

The main goal of series S05 was to capture the creep behaviour of the wall when the direction normal to head joints was loaded (at high temperature) while the direction normal to bed joints was constrained. The temperature evolutions for the HF and CF were similar to those presented in Fig. 17. Fig. 20 shows the evolution of the reaction forces f_{head} and f_{bed} of specimen S05-01 during all steps. The force–displacement diagram and the displacement–time diagram, during loading, holding, and unloading steps are shown in Fig. 21. For this series, only one specimen was tested and its relative behaviour was similar to that of S04.

From the displacement - time diagram, it is possible to observe the primary and secondary creep stages. The total strain, ε_t in the wall by the end of load application was around 0.004. This value is slightly smaller when compared to S04 (by the end of load application) and much higher when compared with series S02. The value of ε_t reached 0.014 by the end of holding. It should be noted that in case of test series S04 and S05, the increase in ε_t during the holding time was almost equal.

4.6. S06: Biaxial creep behaviour

The main objective of test series S06 was to investigate the creep behaviour of the wall under in-plane biaxial compression load at high temperature ($\sigma_{bed}/\sigma_{head} \approx 1$). The HF and CF temperature evolutions were similar to those presented in Fig. 17. Fig. 22 shows the recorded reaction forces f_{head} and f_{bed} for specimen S06-01 during loading, holding, and unloading.

Fig. 23 shows the resulting force–displacement diagrams and the displacement - time diagrams in both directions during all steps for the two specimens. Good agreement between tests can be observed. During load application, a nonlinear displacement stiffening, due to the gradual closure of joints was observed in both directions. The maximum displacement in the direction normal to bed joints was higher as compared to that in the direction normal to head joints due to the difference between the number of bed and head joints in the wall. Similar to biaxial behaviour at room temperature, displacement at the end of the

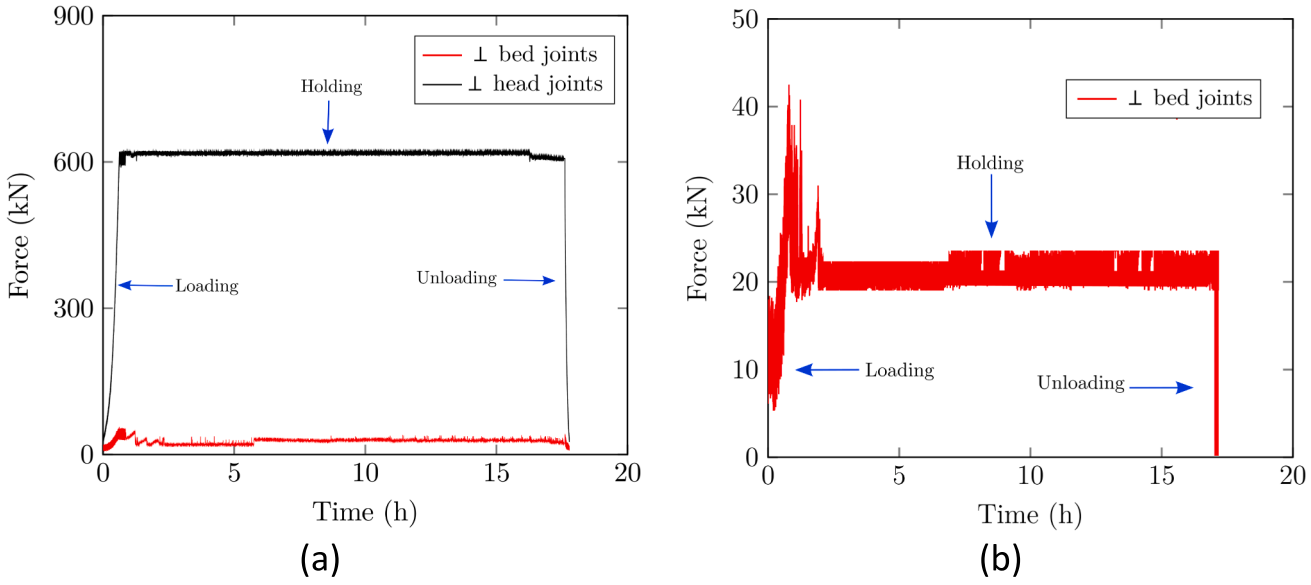

Fig. 20. Specimen S05-01: recorded reaction forces during mechanical loading, holding, and unloading stages: a) in the directions normal to the bed and head joints; b) in the direction normal to the bed joints.

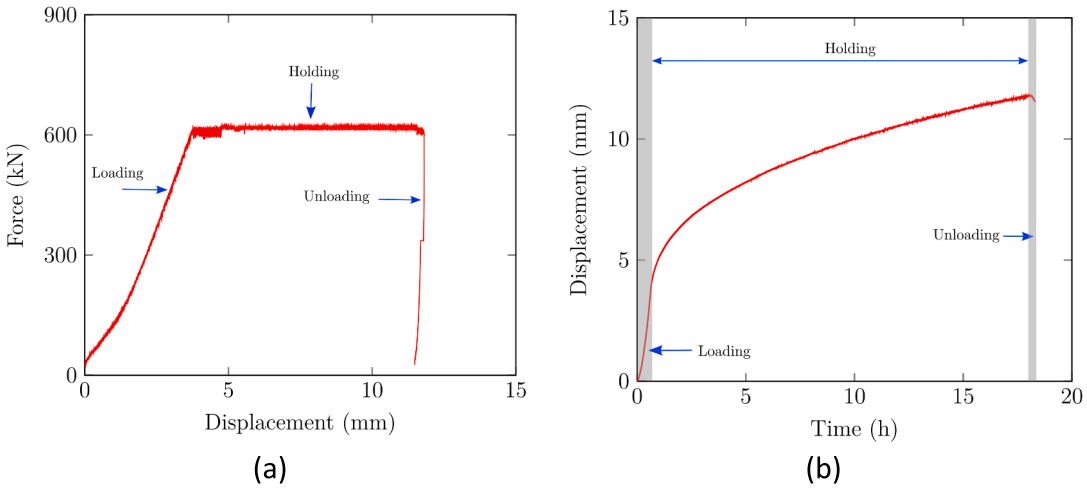

Fig. 21. Test series S05: a) resulting force–displacement diagram; b) time variations of the average displacement during mechanical loading, holding, and unloading steps in the direction normal to the surfaces of head joints.

loading observed are considerably lower compared to the uniaxial tests due to shear interaction at the joints. Moreover, it is interesting to observe that, for the wall subjected to biaxial creep, the increase in the strain rate during the primary stage of creep is similar to the observations made during uniaxial creep. However, during the observed secondary creep stage, the strain rate is considerably lower compared to S04 and S05.

The observed displacements in this test series as well as in S04 and S05 are representative of combined action of mechanical response of material, creep behaviour, interaction between the joints and load transfer mechanism between HF and CF. Due to thermal gradient and thermal expansion, HF of the masonry will experience loading first (due to increased contact with loading plungers). However, due to reduced stiffness, HF will undergo elastic–plastic and viscoplastic deformation, consequently transferring load to the CF.

4.7. S07: Biaxial relaxation behaviour

The goal of test series S07 was to investigate the relaxation behaviour of the wall (constant strain loading conditions). Therefore, at high temperatures and after reaching thermal steady state, a biaxial compression load was applied to both directions normal to bed and head joints. Then, the positions of the movable plungers were locked. In general, the testing procedure of series S07 is similar to S06. The only difference is that the two hydraulic cylinders were kept under displacement control during holding. The temperature evolutions of the HF and CF were like those presented in Fig. 17. Due to a problem during the test, it was not possible to record the displacements of the LVDTs, only reaction forces were recorded.

In these tests, two loading cycles were performed. For the first loading cycle, the wall was loaded up to 4 MPa (in both directions) and then the plungers were blocked (under displacement control) for several hours and the resulting reaction forces were measured. Next, the wall was unloaded and loaded directly up to 6 MPa biaxial compression load. Then, the plungers were blocked for several hours and the reaction forces were recorded. Finally, the wall was unloaded. Fig. 24a shows the recorded reaction forces in both directions during the first and second loading cycles. During loading, the recorded reaction forces increased

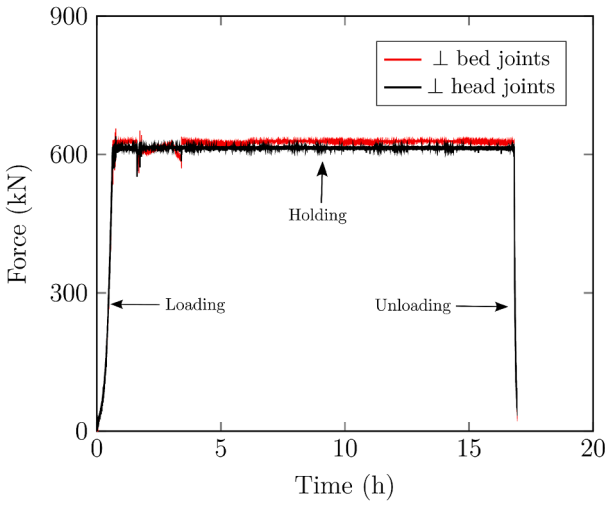

Fig. 22. Specimen S06-01: recorded reaction forces in the directions normal to the surfaces of bed and head joints during mechanical loading, holding, and unloading stages.

gradually to reach the applied peak load. Then, when the position of the plungers is locked, a decay in the resulting reaction forces was observed due to the relaxation behaviour of the wall. At the beginning of the holding, a significant decrease in the reaction forces can be observed. Similar behaviour was noticed for both loading cycles.

It was not possible to keep the same test procedure for the two performed tests, regarding the holding periods. For the second test, the holding period of first loading cycle was shorter compared to the first test and the holding period of the second cycle was longer. Nevertheless, similar trends during loading, holding, and unloading were observed (Fig. 24b).

Stress relaxation of the material can be defined with the same creep law of the material. Similar to the creep, increased rate of stress reduction can be observed during the initial stage of holding and thereafter a constant rate of stress reduction can be observed till the end of the holding stage.

After ending the high temperature creep tests, cooling the walls, and uncovering them, some interesting observations were made, namely: high viscoplastic deformation of the bricks, fusion of the bricks together and perfect closure of joints, and some cracks located near the moving ceramic plungers. Fig. 25 presents an example of a refractory masonry wall after a creep test at 1500 °C. The zone marked in red indicates the locations of closed joints (after testing), while the region marked in blue shows the locations of cracked bricks. The zone in purple indicates the locations of highly deformed bricks. Such bricks were also found in the red zone.

Some examples of perfect closure of head and bed joints are given in Fig. 25b and c. Perfect closure of head joint is depicted in Fig. 25b and perfect closure of both bed and head joint is illustrated in Fig. 25c. Due to the high temperature and the thermomechanical load, the bricks were fused and the joints did not reopen after unloading. Most of the bricks in the wall showed this behaviour. Due to the fusion of the brick and the perfect closure of joints, the recovered displacement after unloading was very small as compared to the recorded displacement during the load application step (as presented earlier).

Near the two moving plungers (region in blue), cracks in the middle of the bricks were observed. Due to the chamfer in the ceramic plungers (Fig. 25e), only half of the brick in contact with the chamfer was loaded. This led to nonuniform loading conditions and stress concentrations at the middle of the brick. The pink marks in the bricks (near the ceramic plungers) were caused by the interaction between the soft insulation and the surfaces of the bricks. At high temperatures, the soft insulation melted and interacted with the bricks leading to a change in bricks' colour.

5. Conclusions

The literature survey on the experimental work of masonry with dry joints has shown that there are very limited available experimental studies on the thermomechanical behaviour of refractory masonry (only two studies) and the understanding of their mechanical behaviour is limited. Therefore, to improve our understanding of the mechanical and thermomechanical behaviour of these structures, a large-scale experimental campaign has been carried out within the framework of the ATHOR Network. In total, 7 large-scale test series (compromising 13 tests) have been performed. Each test series aimed at investigating specific features.

To understand the mechanical behaviour of the masonry at room temperature under cyclic mechanical loading and unloading and to investigate the influence of joints closure and reopening on the mechanical behaviour, cyclic in-plane uniaxial and biaxial compression tests have been performed. The results indicated that the masonry has orthotropic mechanical behaviour and the effective stiffness in the

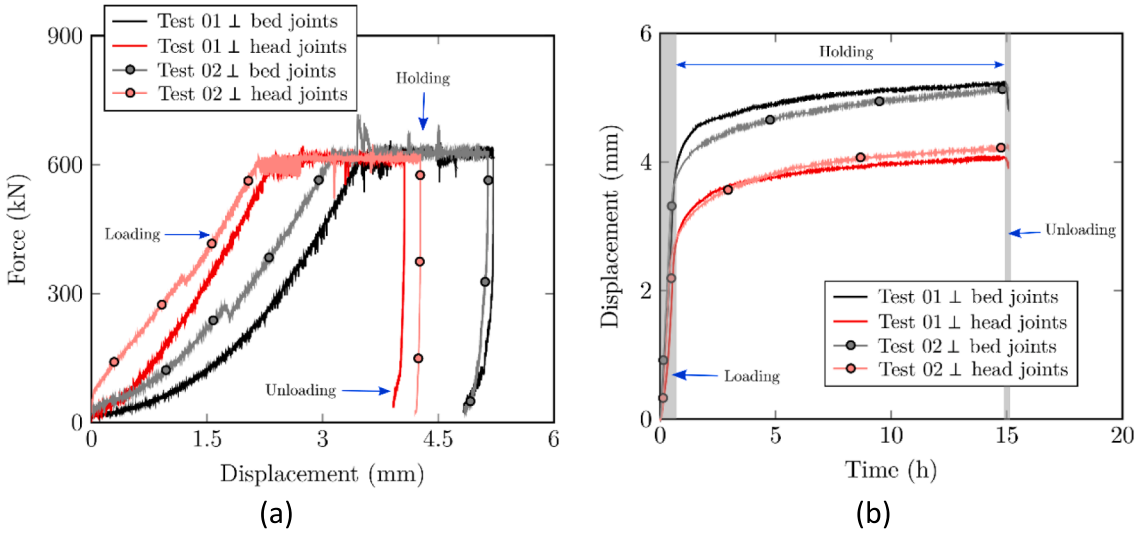

Fig. 23. Test series S06: a) resulting force–displacement diagrams; b) evolution of the average displacements during mechanical loading, holding, and unloading steps in the directions normal to the surfaces of bed and head joints.

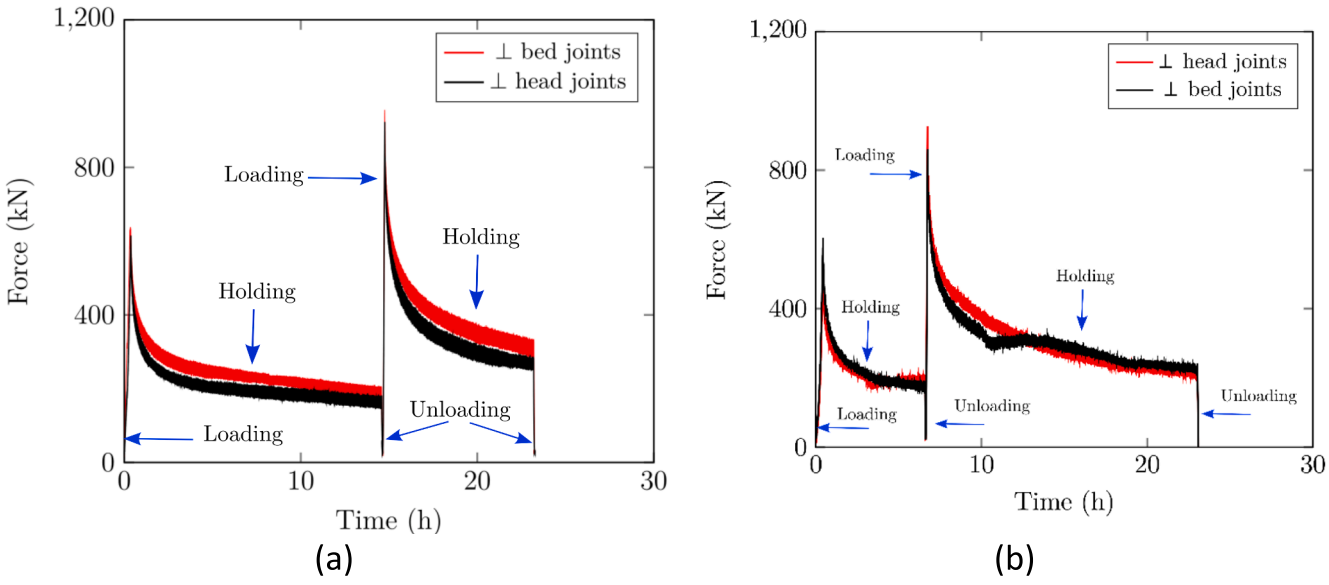

Fig. 24. Forces versus time during loading, holding, and unloading steps of the two performed cycles: a) specimen S07-01; b) specimen S07-02.

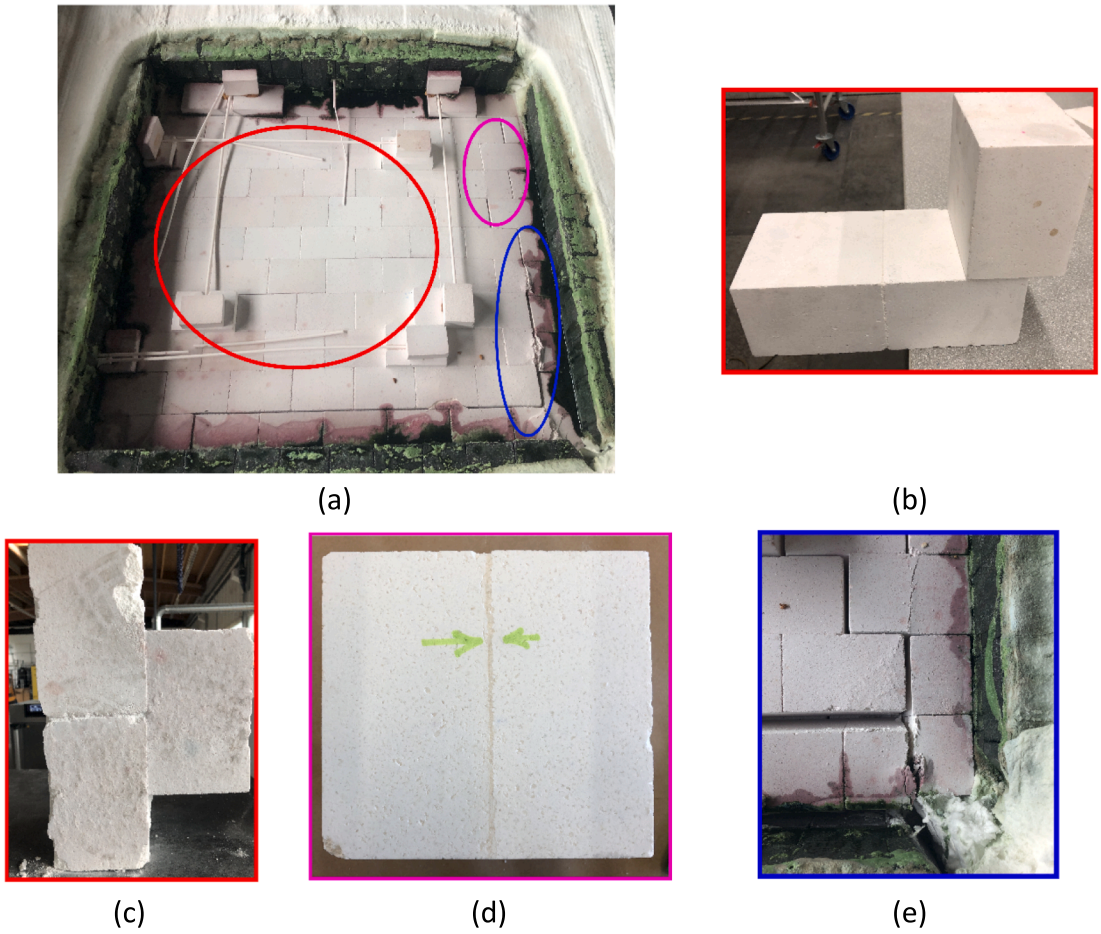

Fig. 25. An example of refractory masonry wall after creep test at 1500 °C: a) global view; b) perfect closure of head joint, two bricks are fused; c) perfect closure of bed and head joints, three bricks are fused; d) deformation of the bricks, the green arrows highlight the high deformation at the middle of the brick; e) cracks due to stress concentration. (For interpretation of the references to colour in this figure legend, the reader is referred to the web version of this article.)

direction normal to head joints is higher than that in the direction normal to bed joints (for the studied walls, the number of head joints was smaller than the number of bed joints). In addition, it has been shown that the stress–strain relationship of the masonry is highly nonlinear (strain stiffening behaviour) due to the gradual closure of joints and the increase of the effective stiffness with joints closure. Moreover, it has been clearly demonstrated that there was permanent deformation after unloading, and the walls did not recover their initial configuration. This behaviour was attributed to the fact that the final joints' thickness after unloading is usually smaller when compared to the initial one (before load application).

The refractory linings usually operate at high temperatures (around 1500 °C) and, at this temperature, the influence of creep and stress relaxation is significant. Therefore, it was essential to test refractory masonry at temperatures similar to those in-services. The in-plane uniaxial, biaxial creep and biaxial stress relaxation behaviour were investigated at 1500 °C. It was observed that during load application, the masonry has strain stiffening nonlinear orthotropic behaviour due to the gradual closure of joints. However, during the holding period and after joints' closure, the behaviour was isotropic (the increase in the creep strain during the holding period was almost similar in the directions normal to bed and head joints). When joints are closed, the wall has a behaviour similar to that of the bricks. Therefore, the creep strains in the directions normal to bed and head joints are the same. After unloading, the experimental results indicated that the recovered strain was very small compared to the strain due to load application. This was attributed to the fact that, during unloading, only a few joints reopen, and their final thickness is very small compared to the initial joint thickness. Secondly, the permanent deformation is also caused by the viscoplastic behaviour of the structure at high temperatures. At high temperature, perfect closure of bed or head or both joints were achieved, and some bricks were fused.

CRediT authorship contribution statement

Mahmoud Ali: Conceptualization, Investigation, Validation, Formal analysis, Writing – original draft. **Rafael L.G. Oliveira:** Conceptualization, Investigation, Validation, Formal analysis, Writing – original draft. **João M. Pereira:** Conceptualization, Investigation, Validation, Writing – review & editing, Supervision, Project administration, Funding acquisition. **João P. Rodrigues:** Validation, Writing – review & editing, Supervision. **Paulo B. Lourenço:** Validation, Writing – review & editing, Supervision, Project administration, Funding acquisition. **Hans Ulrich Marschall:** Conceptualization, Validation, Writing – review & editing, Funding acquisition. **Thomas Sayet:** Conceptualization, Validation, Writing – review & editing, Supervision, Project administration, Funding acquisition. **Alain Gasser:** Conceptualization, Validation, Writing – review & editing, Supervision, Project administration, Funding acquisition. **Eric Blond:** Conceptualization, Validation, Writing – review & editing, Supervision, Project administration, Funding acquisition.

Declaration of Competing Interest

The authors declare that they have no known competing financial interests or personal relationships that could have appeared to influence the work reported in this paper.

Data availability

Data will be made available on request.

Acknowledgements

This work was supported by the funding scheme of the European Commission, Marie Skłodowska-Curie Actions Innovative Training Networks in the frame of the project ATHOR - Advanced THermo-mechanical multi-scale mOdelling Refractory linings 764987 Grant. The second, third and fifth author also acknowledge the financial support by FCT / MCTES through national funds (PIDDAC) under the R&D Unit Institute for Sustainability and Innovation in Structural Engineering (ISISE), under reference UIDB / 04029/2020.

References

[1] J.A. Thamboo, T. Zahra, R. Dhanasekar, Development of design methodology for mortarless masonry system: Case study – a resettlement housing colony, J. Build. Eng. 27 (2020), 100973, https://doi.org/10.1016/J.JOBE.2019.100973.
[2] F. Al Nahhas, R. Ami Saada, G. Bonnet, P. Delmotte, Resistance to fire of walls constituted by hollow blocks: Experiments and thermal modeling, Appl. Therm. Eng. 27 (1) (2007) 258–267.
[3] R.L.G. Oliveira, J.P.C. Rodrigues, J.M. Pereira, P.B. Lourenço, H.U. Marschall, Thermomechanical behaviour of refractory dry-stacked masonry walls under uniaxial compression, Eng. Struct. 240 (2021), 112361, https://doi.org/10.1016/j.engstruct.2021.112361.
[4] D. Ramanenka, M.-L. Antti, G. Gustafsson, P. Jonsén, Characterization of high-alumina refractory bricks and modelling of hot rotary kiln behaviour, Eng. Fail. Anal. 79 (2017) 852–864, https://doi.org/10.1016/j.engfailanal.2017.04.038.
[5] D. Ramanenka, G. Gustafsson, P. Jonsén, Influence of heating and cooling rate on the stress state of the brick lining in a rotary kiln using finite element simulations, Eng. Fail. Anal. 105 (2019) 98–109, https://doi.org/10.1016/j.engfailanal.2019.06.031.
[6] A.M. D'Altri, V. Sarhosis, G. Milani, J. Rots, S. Cattari, S. Lagomarsino, E. Sacco, A. Tralli, G. Castellazzi, S. de Miranda, Modeling Strategies for the Computational Analysis of Unreinforced Masonry Structures: Review and Classification, Arch. Comput. Meth. Eng. 27 (2020) 1153–1185, https://doi.org/10.1007/S11831-019-09351-X/FIGURES/20.
[7] S. Jin, H. Harmuth, D. Gruber, Compressive creep testing of refractories at elevated loads—Device, material law and evaluation techniques, J. Eur. Ceram. Soc. 34 (2014) 4037–4042, https://doi.org/10.1016/J.JEURCERAMSOC.2014.05.034.
[8] S. Samadi, S. Jin, H. Harmuth, Combined damaged elasticity and creep modeling of ceramics with wedge splitting tests, Ceram. Int. 47 (2021) 25846–25853, https://doi.org/10.1016/J.CERAMINT.2021.05.315.
[9] E. Blond, A.K. Nguyen, E. de Bilbao, T. Sayet, A. Batakis, Thermo-chemo-mechanical modeling of refractory behavior in service: Key points and new developments, Int. J. Appl. Ceram. Technol. (2020) 1–8, https://doi.org/10.1111/ijac.13499.
[10] J.J. Coz Díaz, F.R. Mazón, P.J. García Nieto, F.J. Suárez Domínguez, Design and finite element analysis of a wet cycle cement rotary kiln, Finite Elem. Anal. Des. 39 (2002) 17–42, https://doi.org/10.1016/S0168-874X(02)00059-8.
[11] J. Qi, W. Yan, Z. Chen, S. Schafföner, W. Zhou, G. Li, Q. Wang, Preparation and characterization of microporous mullite-corundum refractory aggregates with high strength and closed porosity, Ceram. Int. 46 (2020) 8274–8280, https://doi.org/10.1016/j.ceramint.2019.12.056.
[12] C.A. Schacht, Refractory Linings:, Thermomechanical Design and Applications, Mechanical Engineering Series 95, Eur. J. Eng. Educ. 20 (1995) 386, https://doi.org/10.1080/03043799508928290.
[13] M. Ali, T. Sayet, A. Gasser, E. Blond, Transient Thermo-Mechanical Analysis of Steel Ladle Refractory Linings Using Mechanical Homogenization Approach, Ceramics 2020, Vol. 3, Pages 171-189. 3 (2020) 171–188. 10.3390/ceramics3020016.
[14] V.I. Shubin, Mechanical effects on the lining of rotary cement kilns, Refract. Ind. Ceram 42 (2001) 245–250, https://doi.org/10.1023/A:1012354919912.
[15] S. Samadi, S. Jin, D. Gruber, H. Harmuth, S. Schachner, Statistical study of compressive creep parameters of an alumina spinel refractory, Ceram. Int. 46 (2020) 14662–14668, https://doi.org/10.1016/j.ceramint.2020.02.267.
[16] D. Gruber, H. Harmuth, Thermomechanical behavior of steel ladle linings and the influence of insulations, Steel Res. Int. 85 (4) (2014) 512–518.
[17] K. Andreev, B. Luchini, M.J. Rodrigues, J.L. Alves, Role of fatigue in damage development of refractories under thermal shock loads of different intensity, Ceram. Int. 46 (2020) 20707–20716, https://doi.org/10.1016/J.CERAMINT.2020.04.235.
[18] M. Ali, T. Sayet, A. Gasser, E. Blond, Computational homogenization of elastic-viscoplastic refractory masonry with dry joints, Int. J. Mech. Sci. 196 (2021), 106275, https://doi.org/10.1016/j.ijmecsci.2021.106275.
[19] F. Asadi, D. André, S. Emam, P. Doumalin, M. Huger, Numerical modelling of the quasi-brittle behaviour of refractory ceramics by considering microcracks effect, J. Eur. Ceram. Soc. 42 (2022) 1149–1161, https://doi.org/10.1016/J.JEURCERAMSOC.2021.11.016.
[20] S. Darban, C. Reynaert, M. Ludwig, R. Prorok, I. Jastrzębska, J. Szczerba, Corrosion of Alumina-Spinel Refractory by Secondary Metallurgical Slag Using Coating Corrosion Test, Materials 2022, Vol. 15, Page 3425. 15 (2022) 3425. 10.3390/MA15103425.
[21] K. Andreev, S. Sinnema, A. Rekik, S. Allaoui, E. Blond, A. Gasser, Compressive behaviour of dry joints in refractory ceramic masonry, Constr. Build. Mater. 34 (2012) 402–408, https://doi.org/10.1016/j.conbuildmat.2012.02.024.
[22] S. Allaoui, A. Rekik, A. Gasser, E. Blond, K. Andreev, Digital image correlation measurements of mortarless joint closure in refractory masonries, Constr. Build. Mater. 162 (2018) 334–344, https://doi.org/10.1016/j.conbuildmat.2017.12.055.

[23] R.L.G. Oliveira, J.P.C. Rodrigues, J.M. Pereira, P.B. Lourenço, H. Ulrich Marschall, Normal and tangential behaviour of dry joints in refractory masonry, Eng. Struct. 243 (2021), 112600, https://doi.org/10.1016/j.engstruct.2021.112600.
[24] T. Zahra, M. Dhanasekar, Characterisation and strategies for mitigation of the contact surface unevenness in dry-stack masonry, Constr. Build. Mater. 169 (2018) 612–628, https://doi.org/10.1016/j.conbuildmat.2018.03.002.
[25] G.G. Chewe Ngapeya, D. Waldmann, Overcome of bed-joint imperfections and improvement of actual contact in dry-stacked masonry, Constr. Build. Mater. 233 (2020), 117173, https://doi.org/10.1016/j.conbuildmat.2019.117173.
[26] G.G. Chewe Ngapeya, D. Waldmann, Experimental and analytical analysis of the load-bearing capacity Pu of improved dry-stacked masonry, J. Build. Eng. 27 (2020), 100927, https://doi.org/10.1016/j.jobe.2019.100927.
[27] H. Ben Ayed, O. Limam, M. Aidi, A. Jelidi, Experimental and numerical study of Interlocking Stabilized Earth Blocks mechanical behavior, J. Build. Eng. 7 (2016) 207–216, https://doi.org/10.1016/j.jobe.2016.06.012.
[28] T. Prietl, Determination of material-specific parameters of refractory materials and linings under uniaxial and biaxial load conditions for the non-ferrous metal industry - in German, Montanuniversität Leoben - Austria, 2006.
[29] T. Prietl, H. Antrekowitsch, A. Triessnig, H. Studnicka, A. Filzwieser, The evaluation of refractory linings thermo-mechanical properties, Proc. – Eur. Metall. Conf., EMC 2005 (3) (2005) 1099–1112.
[30] A. Triessnig, H. Studnicka, T. Prietl, Determination of Thermo-Mechanical Properties at the RHI Refractories Technology Center Leoben, RHI Bull. (2006) 33–37.
[31] T.M.H. Nguyen, E. Blond, A. Gasser, T. Prietl, Mechanical homogenisation of masonry wall without mortar, Eur. J. Mech., A/Solids. 28 (2009) 535–544, https://doi.org/10.1016/j.euromechsol.2008.12.003.
[32] S. Schachner, S. Jin, D. Gruber, H. Harmuth, Three stage creep behavior of MgO containing ordinary refractories in tension and compression, Ceram. Int. (2019), https://doi.org/10.1016/j.ceramint.2018.09.124.
[33] A. Sidi Mammar, D. Gruber, H. Harmuth, S. Jin, Tensile creep measurements of ordinary ceramic refractories at service related loads including setup, creep law, testing and evaluation procedures, Ceram. Int. (2016), https://doi.org/10.1016/j.ceramint.2016.01.056.
[34] ATHOR Refractory Linings - ETN ATHOR, available at: https://www.etn-athor.eu/, (n.d.). https://www.etn-athor.eu/ (accessed May 15, 2020).
[35] J. Blaber, B. Adair, A. Antoniou, Ncorr: Open-Source 2D Digital Image Correlation Matlab Software, Exp. Mech. 55 (2015) 1105–1122, https://doi.org/10.1007/s11340-015-0009-1.
[36] D. Vitiello, Thermo-physical properties of insulating refractory materials, Université de Limoges, 2021. PhD thesis,.
[37] R. Kaczmarek, J.C. Dupre, P. Doumalin, O. Pop, L. Breder-Teixeira, J. Gillibert, E. Blond, M. Huger, Thermomechanical behaviour of an alumina spinel refractory for steel ladle applications, in: UNITECR 2019, Yokohama, Japan, 2019. https://hal-unilim.archives-ouvertes.fr/hal-02533698.